Journal of Cardiovascular Computed Tomography 13 (2019) 21–30

Contents lists available at ScienceDirect

Journal of Cardiovascular Computed Tomography

journal homepage: www.elsevier.com/locate/jcct

Pre-procedural fit-testing of TAVR valves using parametric modeling and 3D printing

Ahmed Hosny[a], Joshua D. Dilley[b], Tatiana Kelil[c], Moses Mathur[d], Mason N. Dean[e], James C. Weaver[f,**], Beth Ripley[g,h,*]

[a] Dana-Farber Cancer Institute, Harvard Medical School, USA
[b] Massachusetts General Hospital, Department of Anesthesia, Critical Care & Pain Medicine, Harvard Medical School, USA
[c] Department of Radiology, Brigham and Women's Hospital, Harvard Medical School, USA
[d] Department of Medicine, Division of Cardiology, University of Washington Medical Center, USA
[e] Department of Biomaterials, Max Planck Institute of Colloids and Interfaces, Germany
[f] Wyss Institute for Biologically Inspired Engineering, Harvard University, USA
[g] Department of Radiology, University of Washington, USA
[h] VA Puget Sound Health Care System, USA

ARTICLE INFO

Keywords:
Aortic stenosis
3D printing
Additive manufacturing
Aortic valve
Multi-material printing
Aortic leaflets
Parametric modeling
3-D printing
Calcifications

ABSTRACT

Background: Successful transcatheter aortic valve replacement (TAVR) requires an understanding of how a prosthetic valve will interact with a patient's anatomy in advance of surgical deployment. To improve this understanding, we developed a benchtop workflow that allows for testing of physical interactions between prosthetic valves and patient-specific aortic root anatomy, including calcified leaflets, prior to actual prosthetic valve placement.

Methods: This was a retrospective study of 30 patients who underwent TAVR at a single high volume center. By design, the dataset contained 15 patients with a successful annular seal (defined by an absence of paravalvular leaks) and 15 patients with a sub-optimal seal (presence of paravalvular leaks) on post-procedure transthoracic echocardiogram (TTE). Patients received either a balloon-expandable (Edwards Sapien or Sapien XT, n = 15), or a self-expanding (Medtronic CoreValve or Core Evolut, n = 14, St. Jude Portico, n = 1) valve. Pre-procedural computed tomography (CT) angiograms, parametric geometry modeling, and multi-material 3D printing were utilized to create flexible aortic root physical models, including displaceable calcified valve leaflets. A 3D printed adjustable sizing device was then positioned in the aortic root models and sequentially opened to larger valve sizes, progressively flattening the calcified leaflets against the aortic wall. Optimal valve size and fit were determined by visual inspection and quantitative pressure mapping of interactions between the sizer and models.

Results: Benchtop-predicted "best fit" valve size showed a statistically significant correlation with gold standard CT measurements of the average annulus diameter ($n = 30$, $p < 0.0001$ Wilcoxon matched-pairs signed rank test). Adequateness of seal (presence or absence of paravalvular leak) was correctly predicted in 11/15 (73.3%) patients who received a balloon-expandable valve, and in 9/15 (60%) patients who received a self-expanding valve. Pressure testing provided a physical map of areas with an inadequate seal; these corresponded to areas of paravalvular leak documented by post-procedural transthoracic echocardiography.

Conclusion: We present and demonstrate the potential of a workflow for determining optimal prosthetic valve size that accounts for aortic annular dimensions as well as the active displacement of calcified valve leaflets during prosthetic valve deployment. The workflow's open source framework offers a platform for providing predictive insights into the design and testing of future prosthetic valves.

Abbreviations: TAVR, Transcatheter aortic valve replacement; CTA, Computed tomography angiogram; TTE, Trans-thoracic echocardiogram; LVOT, left ventricular outflow tract; 3D, 3-dimensional

* Corresponding author. VA Puget Sound Health Care System, Mail Code S-114-RAD 1660, S Columbian Way, Seattle, WA, 98108, USA.
** Corresponding author. Wyss Institute for Biologically Inspired Engineering, Harvard University, 3 Blackfan Cir, Boston, MA, 02115, USA.
E-mail addresses: ahmed_hosny@dfci.harvard.edu (A. Hosny), joshuaddilley@gmail.com (J.D. Dilley), tatiana.kelil3d@gmail.com (T. Kelil), moses.mathur@gmail.com (M. Mathur), mason.dean@mpikg.mpg.de (M.N. Dean), james.weaver@wyss.harvard.edu (J.C. Weaver), beth.ripley2@va.gov (B. Ripley).

https://doi.org/10.1016/j.jcct.2018.09.007
Received 6 June 2018; Received in revised form 2 September 2018; Accepted 29 September 2018
Available online 02 October 2018
1934-5925/ Published by Elsevier Inc. on behalf of Society of Cardiovascular Computed Tomography

Table 1
Benchtop-predicted and clinically implanted valve sizes. Patients are primarily grouped by the presence or absence of a paravalvular leak and secondarily grouped by type of implanted TAVR valve. Experimentally predicted "best fit" valve size is reported, along with the manufacturer's recommended size based on 2D annular measurements and the clinically deployed valve size. CT maximum and minimum diameter, the average diameter and the area were obtained from 2D images using standard TAVR measurement technique.** No recommended size reported.

Prosthetic valve sizing					CT measurements		
Paravalvular Leak?	Valve Type	Benchtop Prediction (diameter)	Manufacturer's Recommendation (diameter)	Actually Deployed (diameter)	CT measurement (mm)	CT ave diameter (mm)	CT area (mm2)
No	Sapien XT	23	23	23	18 × 24	21	330
		23	23	23	20 × 24	22	331
		26	26	26	21 × 29	25	464
		29	29	29	26 × 31	28.5	612
	Sapien	23	26	23	22 × 26	24	400
		23	26	23	19 × 26	22.5	338
		29	29	26	24 × 28.6	26.3	528
	Core Evolut	26	29	29	23 × 27	25	434
		26	26	26	18 × 25	21.5	469
		23	23/26	23	17 × 23	20	303
		23	26	26	18 × 25	21.5	329
	CoreValve	29	31	29	22 × 31	26.5	504
		23	26	29	20 × 25	22.5	356
		29	31	31	26 × 30	28	592
		26	29/31	31	23 × 29	26	518
Yes	Sapien XT	29	29	29	23 × 30	26.5	609
		29	29	26	24 × 27	25.5	426
		23	26	23	20 × 25	22.5	355
		23	23	20	20 × 26	23	390
	Sapien	26	29	26	25 × 28	26.5	565
		29	29	26	24 × 31	27.5	575
		26	26	23	20 × 29	24	424
		29	29	26	24 × 32	28	550
	Core Evolut	26	29	29	21 × 26	23.5	394
	CoreValve	26	26/29	26	20 × 26	23	390
		26	29	29	25 × 25	25	479
		29	34	31	25 × 34	29.5	666
		29	31	31	24 × 31	27.5	559
		29	**	31	29 × 36	32.5	738
	St Jude	26	27	25	21 × 26	23.5	397

1. Introduction

Transcatheter aortic valve replacement (TAVR) is widely established as the most common FDA-approved treatment for patients with severe symptomatic aortic stenosis who are at moderate (or greater) risk for surgical valve replacement.[1–3] Despite its widespread use, a recurring challenge of TAVR is achieving a personalized prosthetic valve fit for every patient. Poor fit may result from unanticipated interactions between the geometry and positioning of a prosthetic valve and a patient's anatomy, and may lead to complications. Oversizing the prosthetic valve can lead to annular rupture, and under-sizing can result in an ineffective seal/paravalvular leak or prosthetic valve embolization. Many studies have attempted to predict ideal prosthetic valve fit based on patient-dependent factors such as annular size, shape, and distribution of calcified deposits.[4–7] However, it is still difficult to predict how an opening valve will interact with a unique individual's anatomy.

3D printing is becoming an important tool in the cardiovascular imager's toolbox,[8,9] offering unique opportunities to tailor surgical procedures to patients through the creation of physical models of patient anatomy derived from routine pre-procedural imaging studies.[10–12] 3D printed models have been shown to decrease the learning curve for difficult procedures and improve pre-procedural planning for cases involving complex 3D anatomy.[13–15] In recent years, 3D printing has expanded beyond just the visualization of anatomy, capitalizing on unique properties of 3D materials to physically interrogate how patient anatomy might respond to proposed surgical interventions.[13,16]

In the study, and as a proof of concept, we utilized 3D printing technology to develop and validate a benchtop workflow to test physical interactions between an expandable custom-designed TAVR valve sizer and patient-specific aortic root anatomy, including the active displacement of calcified aortic leaflets during prosthetic valve opening. This workflow has the potential to help guide the selection of optimal valve size for a given patient and alert the physician to the presence of unfavorable geometric interactions between a patient's anatomy and the artificial valve that could result in procedural complications. Through further feedback with real patient data, this pipeline also offers prospects for a better understanding of the mechanisms and factors underlying successful percutaneous valve placement and may help inform future valve designs not only at the aortic, but at all valvular positions.

2. Materials and methods

2.1. Study population

This IRB approved, retrospective study included 30 subjects who underwent a TAVR procedure at Massachusetts General Hospital between the dates of 1/1/2013 and 12/31/2016. To ensure that the study population contained patients with a range of prosthetic valve fits, subjects in this historical dataset were selected based on the presence (n = 15) or absence (n = 15) of paravalvular leaks (a consequence of inadequate seal between prosthetic valve and patient anatomy). The inclusion criterion for patients with paravalvular leak was the presence of mild, moderate, or severe paravalvular leaks on follow-up transthoracic echocardiograms (TTE) in the 30 days following TAVR. Patients who had a transient paravalvular leak at the time of procedure, but spontaneous resolution on follow-up TTE in the 30 days following the procedure, were excluded from this study. The control group consisted of 15 randomly chosen subjects who underwent TAVR procedure

during the same time-period. The inclusion criterion for the control group was the documented absence of paravalvular leak on TTE during the 30 days following the procedure. Age was as follows: control group, 84.9 ± 5.4 (average ± standard deviation), range 71–91; paravalvular leak group, 84.4 ± 5.3, range 72–92. There were 8 female and 7 male patients in the control group and 9 female and 6 male patients in the paravalvular leak group.

The type of valve placed was not part of the initial inclusion criteria, but was considered after data collection for analysis purposes. 15 subjects received balloon-expandable Edwards Sapien valves (either Sapien or Sapien XT) (Edwards Lifesciences, Irvine, CA, USA), 14 received self-expanding Medtronic valves (CoreValve or Core Evolut) (Medtronic, Dublin, Ireland) and 1 received a self-expanding St. Jude Portico valve (St. Jude Medical, St. Paul, MN, USA) (Table 1). All data were doubly blinded to the size of valve placed, the type of valve, and outcomes (paravalvular leak vs. none).

2.2. CT imaging

Cardiac CT scans were performed per standard department protocol. Axial volumetric prospective electrocardiogram-gated acquisition was performed through the heart over a complete R-R interval (0–95% phase) (SOMATOM Definition FLASH, Syngo, Siemens). Images were reconstructed at 10% intervals across one R-R interval (0–95%) at 1 mm slice thickness using a standard soft tissue kernel (i31f). Pixel spacing was 0.263 × 0.263 mm. Patients received iodinated contrast per departmental protocol. Contrast bolus tracking was performed in all patients with a region of interest in the descending aorta using a 200 Hounsfield unit threshold.

2.3. Translation of DICOM data to 3D printable files

2.3.1. Creation of the aortic root and left ventricular outflow tract

For each subject, the best motion-free dataset in diastole was chosen for aortic leaflet coordinate measurements and creation of the 3D model. Diastole was used as leaflets were closed, allowing for motion-free characterization of their size and shape. The blood pool of the aortic root, annulus, and left ventricular outflow tract (LVOT) was segmented using manually determined threshold values adjusted for each subject to include contrast but exclude the aortic wall and surrounding mediastinal structures (3D Slicer, Brigham and Women's Hospital, Boston MA[17]), as previously described.[18] Blood pool segmentation sets were then converted to 3D printable stereolithography (STL) file formats and exported into computer-aided design (CAD) software (Meshmixer, Autodesk; San Rafael, CA) for further post-processing. A 2 mm thick wall was added to the outside of the blood pool in all models to simulate the aortic wall (average thickness of the aortic wall is 2.3 mm[19]).

2.3.2. Creation of calcified aortic leaflets

Calcified portions of the valves, annulus, and LVOT were easily segmented using thresholding strategies (Fig. 1). In all cases, the calcium Hounsfield units were higher than the contrast-opacified blood pool, allowing for robust separation of these two volumes. In contrast, the thin, non-calcified portions of the leaflets could not be accurately separated from the surrounding contrast-enhanced blood pool since their average thickness in relation to z-slice thickness made them susceptible to volume-averaging (average thickness of un-calcified leaflets is 0.41 mm[20]) (Fig. 1). This rendered Hounsfield unit-based segmentation strategies for non-calcified portions of leaflets impractical. To circumvent this problem, a hybrid strategy was designed whereby leaflets were parametrically modelled based on seven landmark coordinates, measured from the CT data.

2.3.3. Parametric design of aortic valve leaflets

A web-based open source software was developed to parametrically generate leaflets (http://ahmedhosny.github.io/av-generator/) (Supplemental Fig. 1). X, Y and Z coordinates were measured from CT data at 7 locations: the point of coaptation of the leaflets (P0), attachment points at the level of the sinotubular junction (P1-P3), and the basal attachment points for the leaflets (P4-P6) (Fig. 2). These coordinates were then entered into the software, which automatically interpolated curves through the coordinates to create leaflets with a uniform thickness of 0.4 mm. The segmented aortic root and calcified deposits were then imported into the software (as STL files) to confirm appropriate alignment of the generated leaflets with the patient's anatomy. Leaflet shape could then be refined by primary controls (sliders) to correct any alignment issues with the aortic annulus and sinuses of Valsalva. A second set of controls were used to adjust the curves within the generated leaflets to maximize alignment of the leaflets with segmented leaflet calcified deposits (Fig. 2C and D). The leaflets and their associated calcified deposits were then exported as separate STL files (Fig. 3).

2.4. Multi-material 3D printing

Aortic root/LVOT models were printed on a Connex500 multi-material 3D printer (Stratasys, Rehovot, Israel). At each print layer, flexible and rigid material photopolymers of different colors were simultaneously jetted and then UV-cured into a solid model. The materials used for the calcified deposits and the aortic root/leaflets were the rigid white VeroWhitePlus® (RGD835) and the flexible transparent TangoPlus® (FLX930), respectively. These two materials represent the stiffness-flexibility extremes for this specific 3D printer, with an approximately 1000-fold modulus difference – the Vero being approximately 1 GPa and the Tango approximately 1 MPa.[21] All aortic root models were printed at 2x size to circumvent the technical difficulties with printing very thin leaflets as well as to facilitate more accurate sizing estimates (as described hereafter).

2.5. Design of custom sizer

Given that real-time adjustment of the valve was a requirement of our protocol, we designed a 3D printable sizer loosely based on the size specifications of a Sapien XT valve (adjustable diameter ranging across 20–29 mm, with adjustments to 23, 26 and 29 mm; fixed height of 16 mm) (file available for download at https://3dprint.nih.gov/discover/3dpx-007958). The sizer was printed at 2x size to match the 2x 3D printed valve models. The design of the sizer included a central stud and an expandable cylindrical valve. Clockwise and anticlockwise rotation of the central stud expands and contracts the cylindrical valve respectively, thus simulating the opening of the valve to multiple diameters in succession. A one-time use pressure-indicating film (Pressurex-micro®, Sensor Products Inc., USA) was wrapped around the cylindrical valve to map contact pressure between the sizer and the 3D printed aortic models. Pressure mappings were digitally captured and thresholded to obtain a quasi-quantitative contact map. The sizer was printed from rigid material (VeroWhitePlus, modulus of 1 GPa) to ensure that circularity was maintained during deployment in the face of counter-pressure from the aortic models. This is an important aspect of any TAVR prosthesis, as any deformation of the circular geometry of the valve may lead to prosthetic leaflet distortion and altered kinematics.[22] The sizer was not designed to simulate variations in height among prosthetic valves of different diameters, nor did it take into consideration the particular features of other prosthetic valve types (e.g. the hourglass shape of the CoreValve).

2.6. Experimental design/methodology

Benchtop-predicted “best fit” valve size was determined by a single observer (AH) for all 30 subjects using the valve sizer. “Best fit” refers to the observer's subjective decision on the valve size least likely to

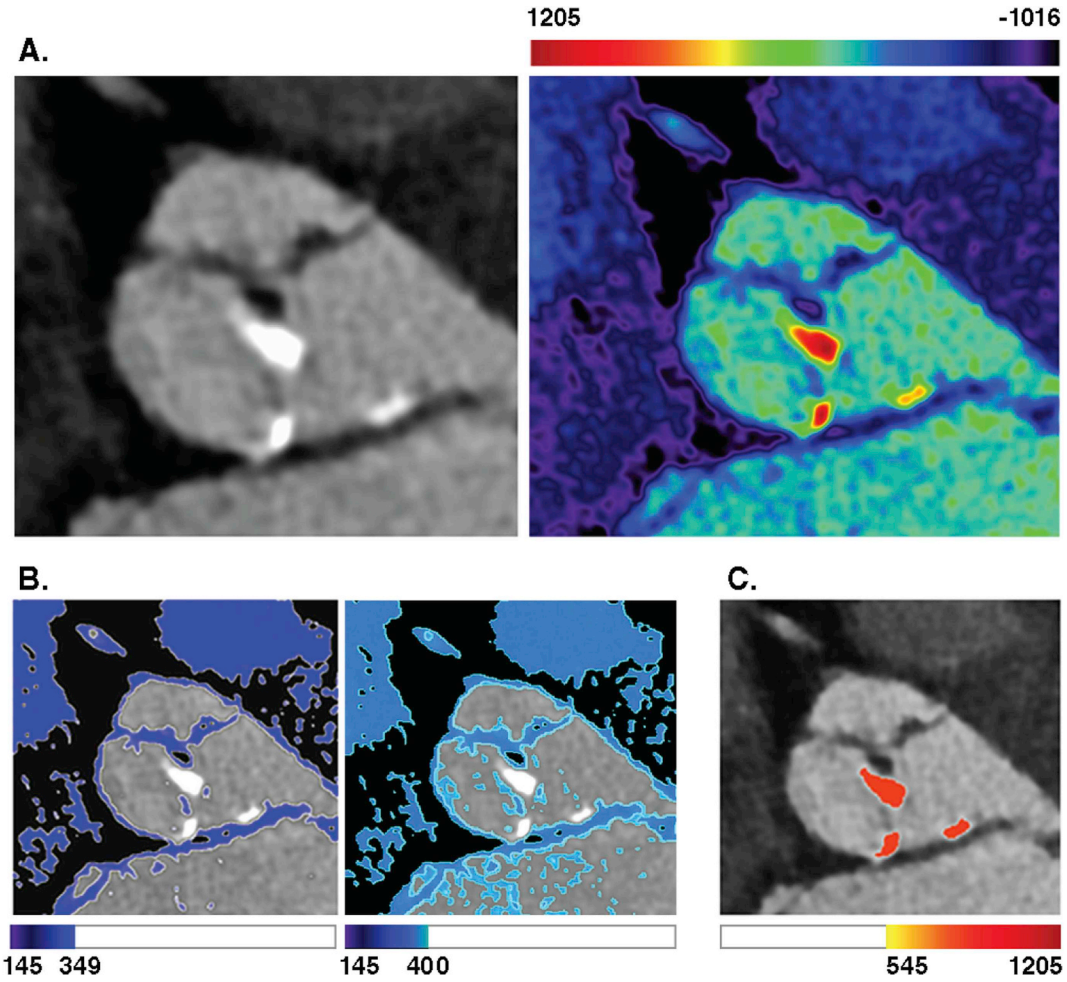

Fig. 1. Segmentation of aortic leaflets is variably challenging. 3D printing requires a segmentation step, wherein voxels are assigned a "keep" or "discard" status depending on the structures of interest. CT data is particularly amenable to threshold-based segmentation strategies based on Hounsfield unit (HU) values. (A) Axial CT image of an aortic valve. The adjacent color map demonstrates the range of HU within the data set, spanning from −1016 to 1205. Choosing a threshold cut-off that includes all non-calcified portions of aortic valve leaflets is challenging due to volume averaging. As seen in panel (A), leaflets have a wide variety of HU, as demonstrated by the variable green and blue. (B) Two different HU cut-offs for segmentation (145–349 HU range and 145–400 HU range). The lower cut-off leads to gaps in the leaflets, while the higher cut-off leads to inclusion of noise in the segmentation. (C) Calcifications have a significantly higher HU that protects against the effects of volume averaging, and are thus easier to segment. (For interpretation of the references to color in this figure legend, the reader is referred to the Web version of this article.)

result in paravalvular leak or annular rupture; this was decided by physically checking for circumferential seal between the sizer and the walls of the aortic root model at each incremental valve size and recording the results (Fig. 4). First, the sizer was placed in a collapsed position within each 3D printed aortic model at the level of the aortic annulus and was adjusted so that it was coaxial with the aortic root, with the valve centered on the aortic annulus so that one half of the valve was above the annular plane and the other was below. Next, the sizer was sequentially opened to 4 different sizes (20, 23, 26 and 29 mm) and areas of inadequate seal (gaps) were recorded by the experimenter for each size. Finally, the "best fit" was determined by reviewing recorded results. Cases where inadequate seal could not be overcome by increasing the valve size were recorded as at risk for paravalvular leak. The experimenter was blinded to the clinically deployed valve size, type (CoreValve, Core Evolut, Sapien, Sapien XT or St. Jude) and outcome (paravalvular leak vs. none).

2.7. Statistics

Wilcoxon matched-pairs signed rank test and Spearman rank sum were used to compare aortic annular measurements made with the sizing device with the average annulus diameter measurements made on 2D CT imaging data sets, as well as to the size of valve clinically implanted. Sensitivity, specificity, and positive predictive value (precision) were determined for prediction of paravalvular leaks.

3. Results

3.1. Accuracy of 3D printed models relative to CT data

Patient-specific 3D printed models were visually compared with CT imaging data to confirm the accuracy of the parametrically generated leaflets (Fig. 5). Next, 3D model annulus accuracy was confirmed by a statistically significant correlation between 3D model annular measurements made with the benchtop sizer and gold standard average annulus diameter measurements made on corresponding 2D CT images by a radiologist with cardiac imaging fellowship training (BR) ($n = 30$, $p < 0.0001$ Wilcoxon matched-pairs signed rank test, Spearman rank sum = 0.877, $p < 0.0001$) (Table 1).

3.2. Benchtop-predicted "best fit" versus clinically determined valve size for balloon-expandable valves

There was agreement between predicted and clinically implanted

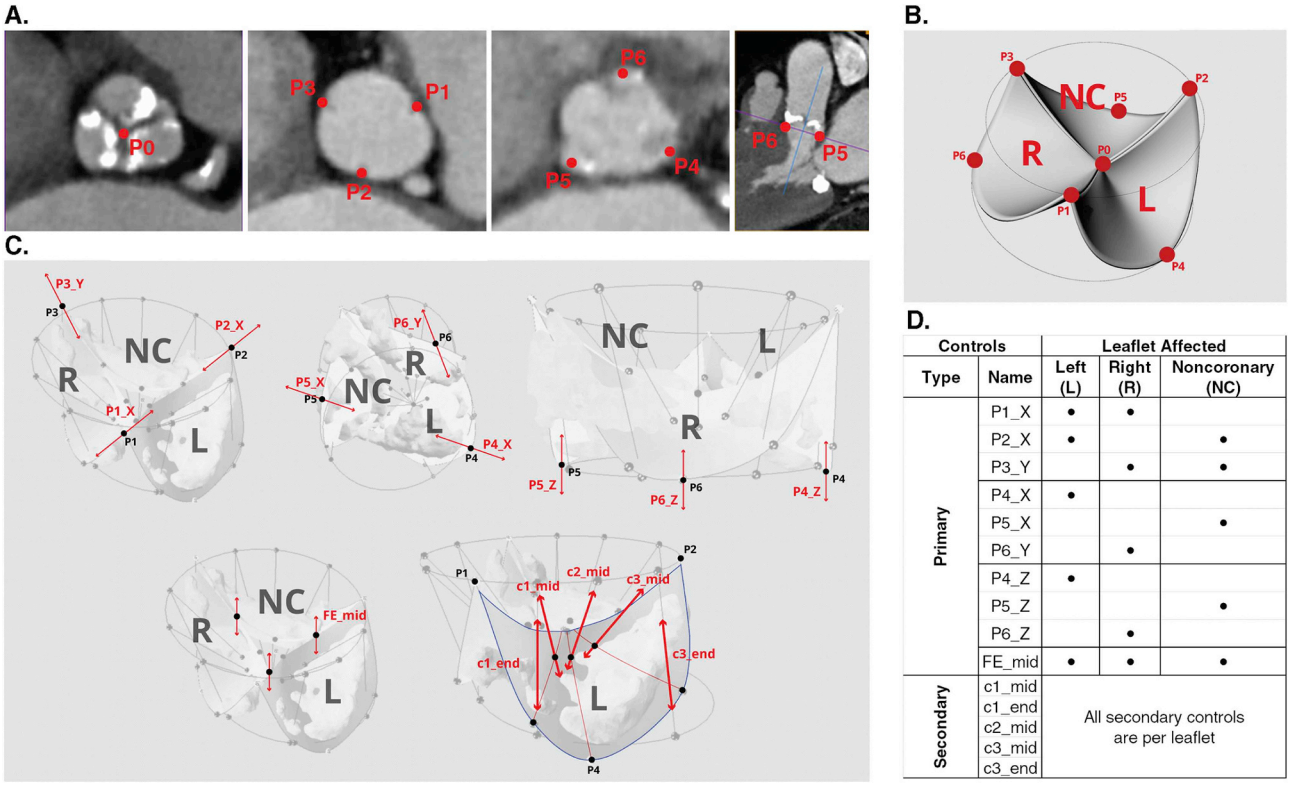

D.

Controls		Leaflet Affected		
Type	Name	Left (L)	Right (R)	Noncoronary (NC)
Primary	P1_X	•	•	
	P2_X	•		•
	P3_Y		•	•
	P4_X	•		
	P5_X			•
	P6_Y		•	
	P4_Z	•		
	P5_Z			•
	P6_Z		•	
	FE_mid	•	•	•
Secondary	c1_mid c1_end c2_mid c3_mid c3_end	All secondary controls are per leaflet		

Fig. 2. Landmark coordinate extraction and parametric leaflet modeling. (A) 3D (x, y and z) coordinates of seven landmark points on aortic leaflets are obtained from CT data. (B) Diagram illustrating relationship between the seven landmark points and the parametric leaflet model. (C) Controls are used to adjust leaflet shape to ensure alignment with the aortic annulus and leaflet calcium. (D) Table illustrating the primary and secondary controls and the corresponding leaflets they affect.

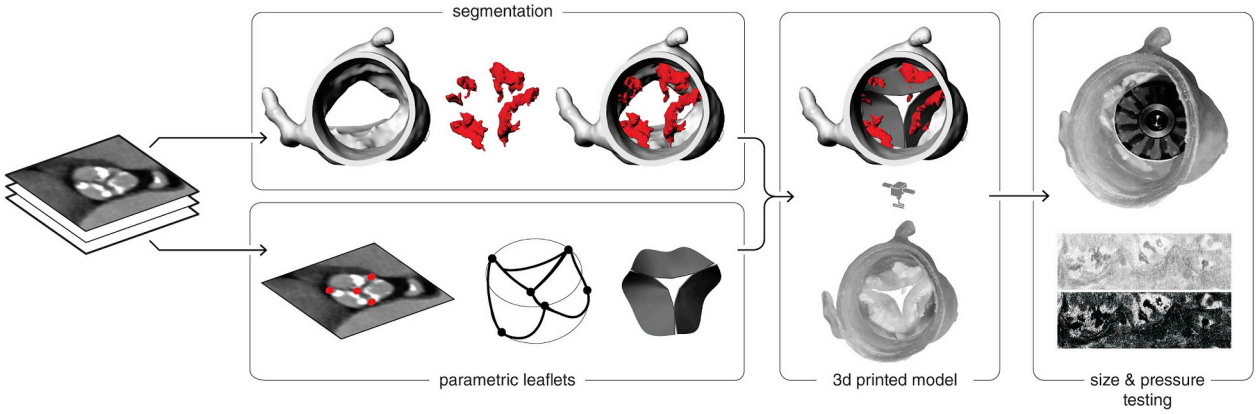

Fig. 3. Diagrammatic illustration of the sizing and leak prediction workflow. The aortic root and leaflet calcifications are segmented from cardiac CTA images and converted into printable mesh files (STL); the underlying leaflets are parametrically created with software, based on landmark coordinates measured from the CTA, and incorporated into the overall model. The patient-specific model is then printed on a multi-material 3D printer. A sizer device is used to simulate multiple prosthetic valve sizes. The probability of a paravalvular leak is predicted by pressure mapping and/or direct observation.

valve size in 9 out of 15 (60%) subjects who received a balloon-expandable valve (P = 0.03 Wilcoxon Rank Sums, Spearman rank sum 0.8769) (Table 1). For all 6 subjects where there was disagreement, the benchtop testing recommended a "best fit" valve size that was larger than the size that was clinically implanted (Table 1). Of note, 5 of those 6 patients developed a paravalvular leak, raising the possibility that the valve was undersized in the clinical scenario.

3.3. Benchtop-predicted "best fit" versus clinically determined valve size for self-expanding valves

There was a match between predicted and clinically implanted valve size in only 5 of the 15 (33%) patients who received a self-expanding valve (CoreValve, Core Evolut or Portico) (Table 1). In all 10 cases of disagreement, the benchtop-predicted "best fit" size was smaller than the implanted size. Because all benchtop measurements were carried out with a sizer designed to mimic an annularly placed valve, the measurements did not take into consideration the upsizing recommendations for the Medtronic valves (necessitated by the supra-annular position of the prosthetic valve). We therefore applied a post-analysis correction factor based on the manufacturer's recommendations to the predicted valve sizes of all subjects that received a Medtronic valve in a secondary analysis. All predictions were upsized by one valve size (e.g. 23 mm upsized to 26 mm, 26 mm upsized to 29 mm, etc). This led to a match between predicted "best fit" and clinically implanted valve size in 10 of the 15 patients who received self-

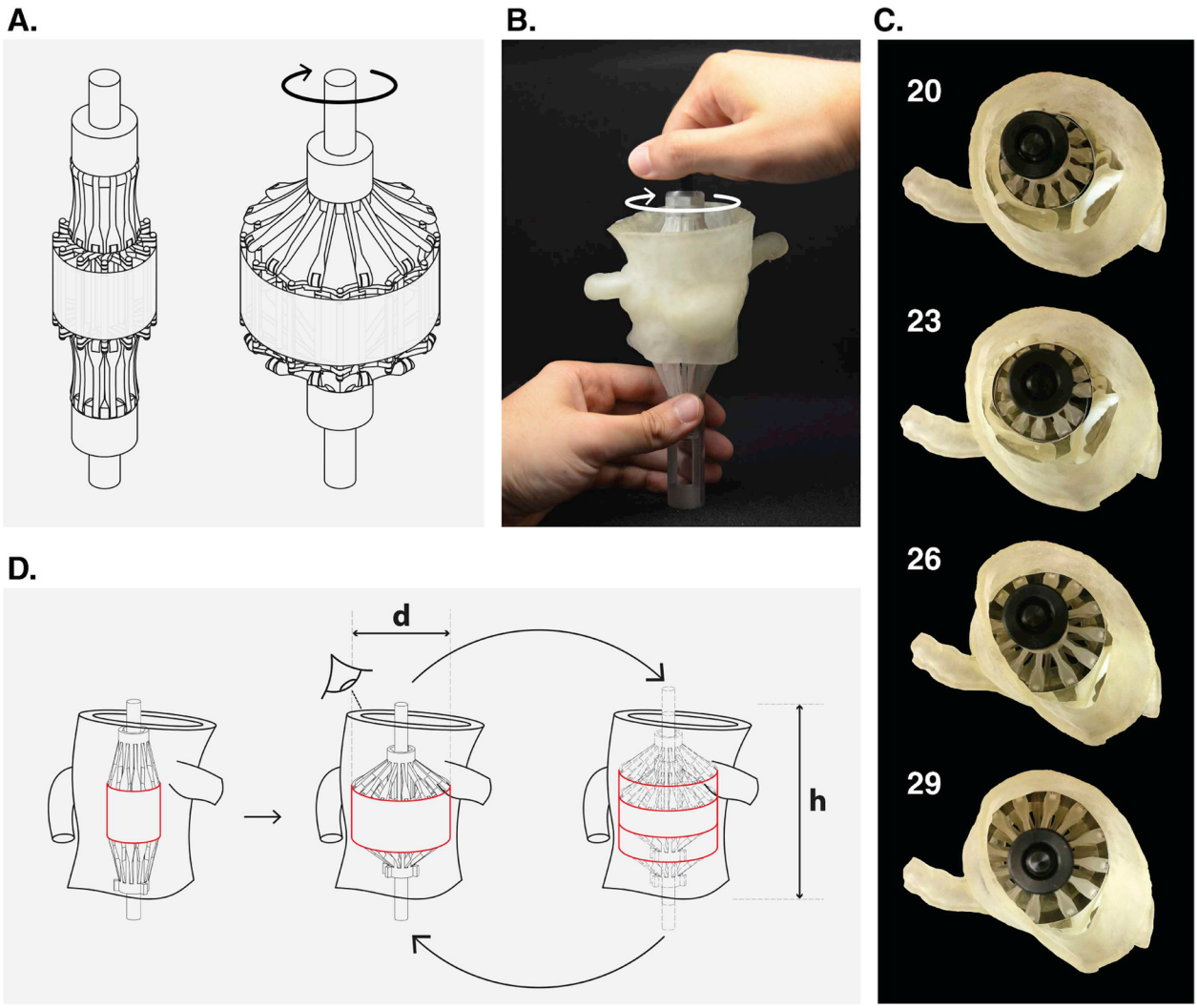

Fig. 4. Sizer device used to simulate TAVR prosthetic. (A) Schematic drawings of the sizer device in both open and closed positions. (B) Sizer inserted into aortic model and set to the desired diameter by rotating a dial. (C) Series of tests performed on an aortic model by expanding the sizer to different diameters. (D) Flowchart illustrating the sizing process where the diameter (d) and vertical alignment (h) are adjusted for best fit.

expanding valves (67%) (improved from the baseline 33% match). We did not apply a correction factor to the predicted "best fit" in the single case of the St. Jude valve, given that the prosthetic valve is located at the annular plane.

3.4. Qualitative prediction of effective seal

At the time of fit testing, predictions were made about which patients were at high risk for inadequate seal and development of a paravalvular leak. This prediction was based on visual evidence of an incomplete seal between the expanded valve sizer and the patient model at the annular plane. Overall, 17 cases were predicted to be negative for leak and 13 cases were predicted to be positive for leak. Predictions were correct in 20 cases (true positive + true negative) and incorrect in 10 cases (false positive + false negative).

Correct predictions (combined true positive and true negative) were made in 11 of 15 subjects who received balloon-expandable valves. The qualitative prediction test had a sensitivity of 75%, specificity of 71%, and positive predictive value of 75% (Table 2). Correct predictions (combined true positive and true negative) of inadequate seal/paravalvular leak were made in 9 of 15 subjects who received self-expanding valves. The qualitative prediction test for this subset of valves had a sensitivity of 43%, specificity of 75%, and positive predictive value of 60% (Table 2).

3.5. Quantitative prediction of effective seal

Topological pressure maps were created in 5 subjects who received balloon-expandable valves (Fig. 6). Dark regions represent contact between the sizer and the model, while light regions denote a lack of contact. Light regions that continued from the top to the bottom edge of the valve sizer (indicating a channel) were identified as potential leak locations. These potential leak locations corresponded with the actual location of leaks as reported on post-procedure TTE (See Fig. 6 legend).

4. Discussion

Here, we report on the performance of a benchtop workflow designed to physically determine optimal TAVR valve size and fit for a unique patient's anatomy. The development of scalable and patient-specific workflows is vital and timely. As TAVR devices and safety improve, the number of patients eligible for this intervention will continue to grow.[1,23–26] Being able to identify intermediate and low risk surgical patients whose anatomy places them at greater probability for TAVR complications is critical. These patients may be better served by surgery, as the risks of an imperfect TAVR result may outweigh the

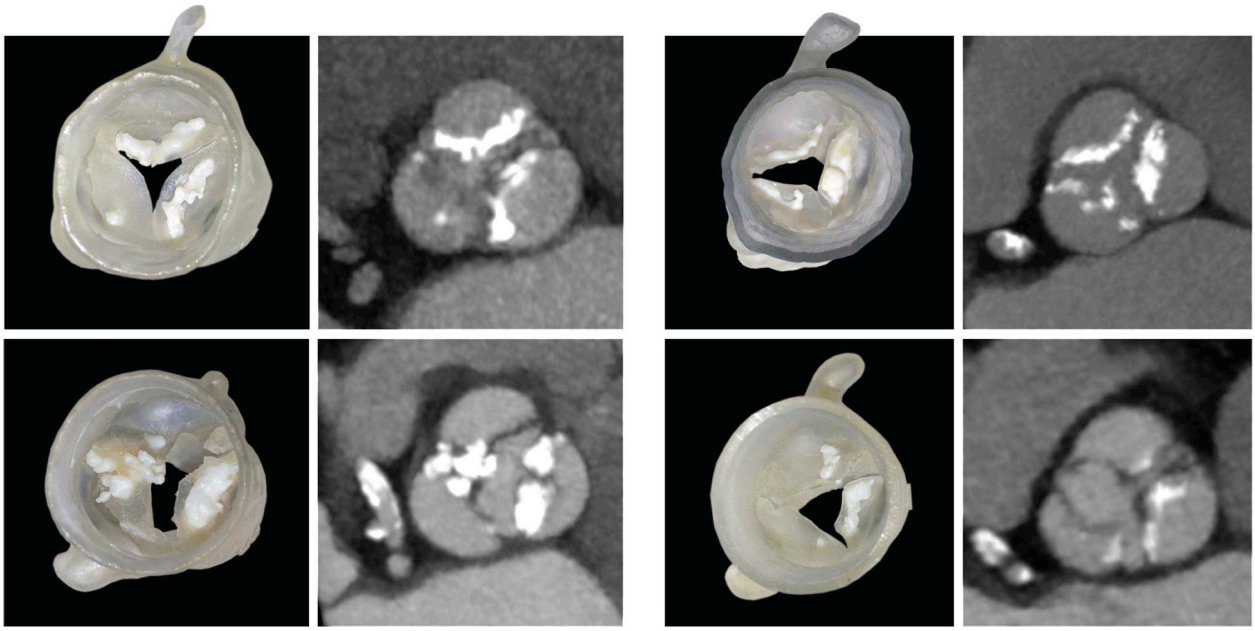

Fig. 5. Examples of 3D printed models and corresponding CT images. Photographs of 3D printed models are on the left and source CT images on the right; CT images are reconstructed in the annular plane; thin MIP (3–5 mm) technique is used to demonstrate calcifications to better effect.

benefits of a minimally invasive approach.

Annular measurements provide an important starting point for determining appropriate valve size, but additional patient-specific factors must be considered. For example, the degree of annular eccentricity and the relative distribution of calcified deposits on valve leaflets and in the LVOT influence valve anchoring and seal.[27–31] It is not known to what extent each of these factors contributes to the final fit. For instance, should the presumed effect of annular eccentricity be weighted more than distribution of calcified deposits or vice versa? A key advantage of our workflow is that it provides a relatively non-ambiguous result that synthesizes anatomical data, such as leaflet calcified deposits, annular size, and annular and LVOT geometry - without needing to determine the relative weighting factors for these different characteristics. For example, the greater disagreement between predicted and clinically implanted balloon-expandable valve sizes in patients with poor fit (62%, defined by presence of paravalvular leak) versus those with good fit (14%, defined by absence of paravalvular leak) suggests that the workflow might have identified problems or aspects of fit with these valves that were not clinically apparent. Given that in all cases of discrepancy, the larger valves were recommended by the benchtop workflow, it is possible and perhaps even likely that the experimentally predicted size would have outperformed the clinically-implanted size by reducing the risk of paravalvular leak.

While our pipeline lays important groundwork for more efficient, patient-specific, and safer TAVR by its design, it can be made inherently more generalizable and effective in future iterations. First, the less accurate predictions for self-expanding relative to balloon-expandable valves can be addressed through the design of additional sizers that more closely match various valve styles and dimensions and incorporate more detailed stent, leaflet, skirt, and sealing cuff designs, or through development of mathematical conversion factors for predictions based on the valve type and degree of upsizing recommended by the manufacturer. Moreover, since the sizer mechanism was constructed parametrically and fabricated as a single piece using additive manufacturing, additional sizers can be rapidly produced based on the desired need of the physician. This flexibility also allows for continued alignment with valve iterations over time. For example, the first and second generation valves evaluated here have largely been replaced by newer models, including the Sapien 3, with enhancements to mitigate paravalvular leaks.[32] Future iterations of the sizer will reflect these design changes.

Second, we created models from aortic roots in diastole to facilitate measurements needed to create aortic leaflets. However, the aortic root is maximally expanded during systole, which could have affected the accuracy of our results. To address this issue, a more thorough understanding of calcified leaflet deformation modes obtained from ex-vivo microCT studies could be used to augment our valve simulation model through the incorporation of a second set of landmark leaflet measurements made during systole.

Third, the actual physical properties of the aortic wall, calcified deposits, and valve were approximated given current limitations in 3D printable materials. While the geometric accuracy of the 3D printed model has been validated, the mechanical properties of the 3D printed materials used in this study are only capable of small scale deformations, falling short of the strain-stiffening behaviour demonstrated by human aortic tissue. More biologically accurate materials[33] will allow improved modeling, including re-creating pressure gradients during flow analysis and quantitatively testing forces that could result in

Table 2
Leak prediction test results. Leak prediction test results for all patients, patients with balloon-expandable valves and patients with self-expanding valves.

Valves	Predictions	Leak Present	Leak Absent	Sensitivity	Specificity	Precision
ALL VALVES	Leak predicted	TP = 9	FP = 4	60%	73%	69%
	No leak predicted	FN = 6	TN = 11			
BALLOON EXPANDABLE	Leak predicted	TP = 6	FP = 2	75%	71%	75%
	No leak predicted	FN = 2	TN = 5			
SELF EXPANDABLE	Leak predicted	TP = 3	FP = 2	43%	75%	60%
	No leak predicted	FN = *4*	TN = 6			

	aortic root models with deployed sizers		pressure mapping data raw (top) thresholded (bottom)
	photographic	radiographic	
A (23mm)	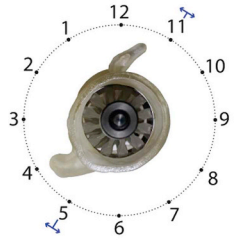		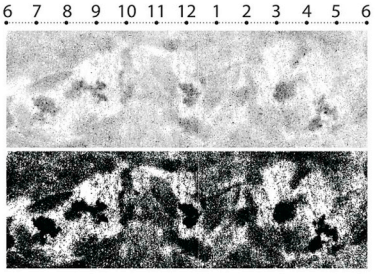
B (23mm)	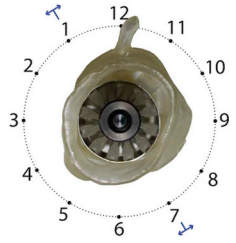	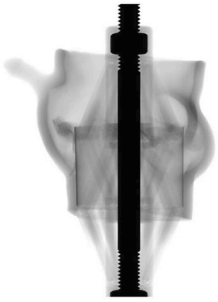	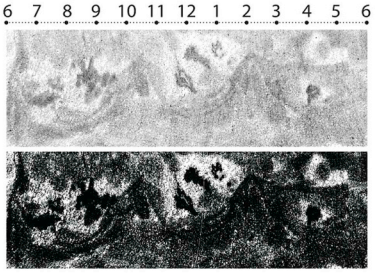
C (26mm)	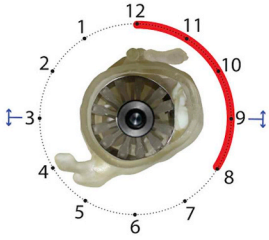	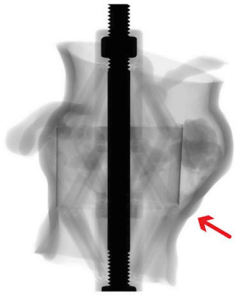	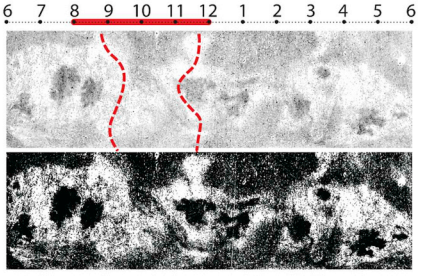
D (29mm)	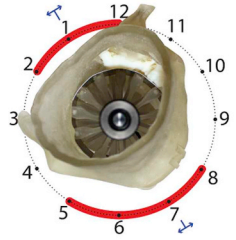	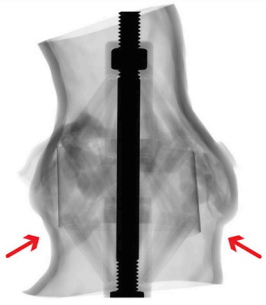	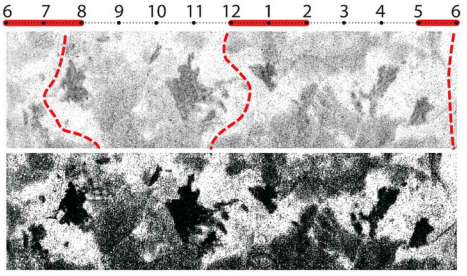
E (26mm)	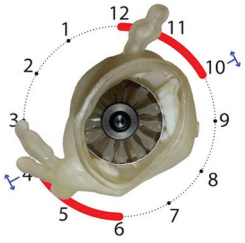	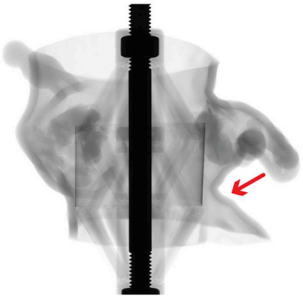	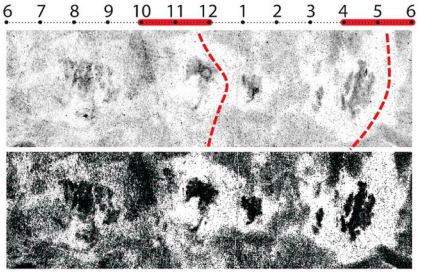

(caption on next page)

Fig. 6. Examples of size and pressure testing. Examples of cases without (A and B) and with (C, D and E) paravalvular leaks. Clock-face positions are used to reference the leak location. Red markings along the hour positions demonstrate confirmed locations of paravalvular leaks, as assessed on post-procedure TTE. Red arrows on the radiographic images depict leak locations qualitatively predicted during experiments. Dashed red lines on the pressure maps demarcate areas of low or no contact pressure that persist from the top edge to the bottom edge of the valve (forming a channel); these are areas where leaks were quantitatively predicted. (For interpretation of the references to color in this figure legend, the reader is referred to the Web version of this article.)

annular rupture. Recent advances in 3D printed metamaterials with micro-structured reinforcements[16,34] and the development of novel photopolymerizable hydrogels pave the way towards achieving these results.[35]

Fourth, our predicted "best fit" was determined by a single observer's observations and was therefore subjective. However, the open cage-like design of the sizer makes it amenable to the addition of real-time sensory elements, which would result in a more objective read-out utilizing pressure mapping and proximity-sensing. Our initial results with quantitative pressure mapping are encouraging and support this presumption.

Finally, the data is limited by the design of the study. It was performed retrospectively with only 30 patients at a single center. The outcome of the procedure is also heavily dependent upon the ability of the individual performing the procedure. Future data will be made more valuable by performing prospective studies that include a larger number of patients and multiple sites.

5. Conclusion

In the present study, we demonstrate that a workflow to physically test biomechanical interactions between a custom-designed TAVR valve sizer and 3D printed patient-specific anatomy is feasible using data obtained from routine pre-procedural cardiac CTA. This workflow may be a useful complement to current clinical sizing strategies and may also help anticipate the most likely complications for an individual's unique anatomy and pathology. In addition, by its very design, our benchtop workflow involves the direct, hands-on interaction between the physician, the 3D printed valve analogue, and a patient's unique anatomy, allowing for a much more intuitive interaction as well as haptic feedback to the physician during simulated valve deployment. In the spirit of innovation, we have made our custom leaflet generation software and the 3D printable valve sizer files open-source and available for download, creating a springboard for evolvable biomedical design that keeps pace with the market's state of the art.

Funding

This work was supported by a grant from the Human Frontier Science Program to MND and JCW under award #HFSP RGY0067.

Disclosures

Authors have no conflicts of interest. Portions of this work are included under U.S. Provisional Patent Application No. 62/419,268 filed November 8, 2016 with assignment to Harvard University.

Acknowledgements

The authors thank Dmitry Levin for comments and feedback on the manuscript.

Appendix A. Supplementary data

Supplementary data to this article can be found online at https://doi.org/10.1016/j.jcct.2018.09.007.

References

1. Thourani VH, Kodali S, Makkar RR, et al. Transcatheter aortic valve replacement versus surgical valve replacement in intermediate-risk patients: a propensity score analysis. *Lancet.* 2016;387(10034):2218–2225.
2. Smith CR, Leon MB, Mack MJ, et al. Transcatheter versus surgical aortic-valve replacement in high-risk patients. *N Engl J Med.* 2011;364(23):2187–2198.
3. Arora S, Strassle PD, Ramm CJ, et al. Transcatheter versus surgical aortic valve replacement in patients with lower surgical risk scores: a systematic review and meta-analysis of early outcomes. *Heart Lung Circ.* 2017;26(8):840–845.
4. Jilaihawi H, Doctor N, Kashif M, et al. Aortic annular sizing for transcatheter aortic valve replacement using cross-sectional 3-dimensional transesophageal echocardiography. *J Am Coll Cardiol.* 2013;61(9):908–916.
5. Condado JF, Corrigan 3rd FE, Lerakis S, et al. Anatomical risk models for paravalvular leak and landing zone complications for balloon-expandable transcatheter aortic valve replacement. *Cathet Cardiovasc Interv.* May 2017. https://doi.org/10.1002/ccd.26987.
6. Wang Q, Sirois E, Sun W. Patient-specific modeling of biomechanical interaction in transcatheter aortic valve deployment. *J Biomech.* 2012;45(11):1965–1971.
7. Auricchio F, Conti M, Morganti S, et al. Simulation of transcatheter aortic valve implantation: a patient-specific finite element approach. *Comput Methods Biomech Biomed Eng.* 2014;17(12):1347–1357.
8. Bramlet M, Olivieri L, Farooqi K, et al. Impact of three-dimensional printing on the study and treatment of congenital heart disease. *Circ Res.* 2017;120(6):904–907.
9. Giannopoulos AA, Steigner ML, George E, et al. Cardiothoracic applications of 3-dimensional printing. *J Thorac Imag.* 2016;31(5):253–272.
10. Matsumoto JS, Morris JM, Foley TA, et al. Three-dimensional physical modeling: applications and experience at mayo clinic. *Radiographics.* 2015;35(7):1989–2006.
11. Mitsouras D, Liacouras P, Imanzadeh A, et al. Medical 3D printing for the radiologist. *Radiographics.* 2015;35(7):1965–1988.
12. Ripley B, Levin D, Kelil T, et al. 3D printing from MRI Data: harnessing strengths and minimizing weaknesses. *J Magn Reson Imag.* 2017;45(3):635–645.
13. Hermsen JL, Burke TM, Seslar SP, et al. Scan, plan, print, practice, perform: development and use of a patient-specific 3-dimensional printed model in adult cardiac surgery. *J Thorac Cardiovasc Surg.* 2017;153(1):132–140.
14. Schmauss D, Schmitz C, Bigdeli AK, et al. Three-dimensional printing of models for preoperative planning and simulation of transcatheter valve replacement. *Ann Thorac Surg.* 2012;93(2):e31–e33.
15. Essayed WI, Unadkat P, Hosny A, et al. 3D printing and intraoperative neuronavigation tailoring for skull base reconstruction after extended endoscopic endonasal surgery: proof of concept. *J Neurosurg. March.* 2018:1–8.
16. Qian Z, Wang K, Liu S, et al. Quantitative prediction of paravalvular leak in transcatheter aortic valve replacement based on tissue-mimicking 3D printing. *JACC Cardiovasc Imaging.* 2017;10(7):719–731.
17. Fedorov A, Beichel R, Kalpathy-Cramer J, et al. 3D slicer as an image computing platform for the quantitative imaging network. *Magn Reson Imaging.* 2012;30(9):1323–1341.
18. Ripley B, Kelil T, Cheezum MK, et al. 3D printing based on cardiac CT assists anatomic visualization prior to transcatheter aortic valve replacement. *J Cardiovasc Comput Tomogr.* 2016;10(1):28–36.
19. Li AE, Kamel I, Rando F, et al. Using MRI to assess aortic wall thickness in the multiethnic study of atherosclerosis: distribution by race, sex, and age. *AJR Am J Roentgenol.* 2004;182(3):593–597.
20. Sahasakul Y, Edwards WD, Naessens JM, et al. Age-related changes in aortic and mitral valve thickness: implications for two-dimensional echocardiography based on an autopsy study of 200 normal human hearts. *Am J Cardiol.* 1988;62(7):424–430.
21. Bartlett NW, Tolley MT, Overvelde JTB, et al. A 3D-printed, functionally graded soft robot powered by combustion. *Science.* 2015;349(6244):161–165.
22. Gunning PS, Vaughan TJ, McNamara LM. Simulation of self expanding transcatheter aortic valve in a realistic aortic root: implications of deployment geometry on leaflet deformation. *Ann Biomed Eng.* 2014;42(9):1989–2001.
23. Bourantas CV, Serruys PW. Evolution of transcatheter aortic valve replacement. *Circ Res.* 2014;114(6):1037–1051.
24. Cribier A, Eltchaninoff H, Tron C, et al. Treatment of calcific aortic stenosis with the percutaneous heart valve: mid-term follow-up from the initial feasibility studies: the French experience. *J Am Coll Cardiol.* 2006;47(6):1214–1223.
25. Frerker C, Bestehorn K, Schlüter M, et al. In-hospital mortality in propensity-score matched low-risk patients undergoing routine isolated surgical or transfemoral transcatheter aortic valve replacement in 2014. *Research in Cardiology.* 2017;106(8):610–617http://link.springer.com/article/10.1007/s00392-017-1097-y.
26. Otto CM, Prendergast B. Aortic-valve stenosis–from patients at risk to severe valve obstruction. *N Engl J Med.* 2014;371(8):744–756.
27. Azzalini L, Ghoshhajra BB, Elmariah S, et al. The aortic valve calcium nodule score (AVCNS) independently predicts paravalvular regurgitation after transcatheter aortic valve replacement (TAVR). *J Cardiovasc Comput Tomogr.* 2014;8(2):131–140.
28. Khalique OK, Hahn RT, Gada H, et al. Quantity and location of aortic valve complex

calcification predicts severity and location of paravalvular regurgitation and frequency of post-dilation after balloon-expandable transcatheter aortic valve replacement. *JACC Cardiovasc Interv.* 2014;7(8):885–894.
29. Freeman M, Webb JG, Willson AB, et al. Multidetector CT predictors of prosthesis–patient mismatch in transcatheter aortic valve replacement. *J Cardiovasc Comput Tomogr.* 2013;7(4):248–255.
30. Buellesfeld L, Stortecky S, Heg D, et al. Extent and distribution of calcification of both the aortic annulus and the left ventricular outflow tract predict aortic regurgitation after transcatheter aortic valve replacement. *EuroIntervention.* 2014;10(6):732–738.
31. Wong DTL, Bertaso AG, Liew GYH, et al. Relationship of aortic annular eccentricity and paravalvular regurgitation post transcatheter aortic valve implantation with CoreValve. *J Invasive Cardiol.* 2013;25(4):190–195.
32. Yang T-H, Webb JG, Blanke P, et al. Incidence and severity of paravalvular aortic regurgitation with multidetector computed tomography nominal area oversizing or undersizing after transcatheter heart valve replacement with the sapien 3. *JACC Cardiovasc Interv.* 2015;8(3):462–471.
33. Khanafer K, Duprey A, Zainal M, et al. Determination of the elastic modulus of ascending thoracic aortic aneurysm at different ranges of pressure using uniaxial tensile testing. *J Thorac Cardiovasc Surg.* 2011;142(3):682–686.
34. Wang K, Wu C, Qian Z, et al. Dual-material 3D printed metamaterials with tunable mechanical properties for patient-specific tissue-mimicking phantoms. *Additive Manufacturing.* 2016;12(Part A):31–37.
35. Hockaday LA, Kang KH, Colangelo NW, et al. Rapid 3D printing of anatomically accurate and mechanically heterogeneous aortic valve hydrogel scaffolds. *Biofabrication.* 2012;4(3):035005.